Fragment-mass distributions in ^{16}O-induced reactions at energies well above the Coulomb barrier

K. Atreya,[1,2] A. Sen,[1,2] D. Paul,[1,2] T. K. Ghosh,[1,2,*] Kavita Rani,[1] Md. Moin Shaikh,[1,†] K. Banerjee,[1,2] C. Bhattacharya,[1,2] Samir Kundu,[1,2] S. Manna,[1,2] G. Mukherjee,[1,2] S. Nandi,[1,‡] R. Pandey,[1,2] T. K. Rana,[1,2] Pratap Roy,[1,2] S. Mukhopadhyay,[1,2] and Raj Kumar Santra[1]

[1]*Variable Energy Cyclotron Centre, 1/AF, Bidhan Nagar, Kolkata 700064, India*

[2]*Homi Bhabha National Institute, Training School Complex, Anushakti Nagar, Mumbai - 400094, India*

(Received 11 January 2024; accepted 23 May 2024; published 21 June 2024)

Background: The excitation energy dependence of the fission fragment mass distributions for heavy ion-induced reactions on preactinides targets well above the Coulomb barrier energies has received limited attention due to the lack of data. An extensive study is required to understand the reaction mechanism at high excitation energy as it bridges our understanding of the mechanism of fission and noncompound nuclear reactions.

Purpose: The purpose was to understand the fusion-fission dynamics well above the Coulomb barrier energies, particularly to address if the theoretical models that are valid near the Coulomb barrier can explain the fission data at high excitation energies.

Methods: In the experiment, a pulsed heavy-ion beam from the cyclotron was utilized, and the resulting binary fragments were detected using two position-sensitive multiwire proportional counters. By analyzing the time-of-flight differences and position information (θ, ϕ) of the binary fragments, mass distributions were obtained for the reactions ^{16}O + ^{181}Ta, ^{197}Au, ^{205}Tl, and ^{208}Pb.

Results: The variance of the fission fragment mass distributions exhibits a smooth increase with excitation energy, although values are smaller compared to the predicted values of the semiempirical calculation GEF. The measured variation of the variance of the mass distribution with the fissility showed an exponential increase. The contribution of fast fission have been identified at high energies with mass asymmetry value ≈ 0.22.

Conclusion: Our systematic measurements over a wide range of excitation energy and target mass indicate that the fission fragment mass distributions are consistent with statistical models up to $\approx$2 times the Coulomb barrier energies for the pre-actinides target nuclei when bombarded with ^{16}O. The result provides benchmark data to test the new reaction models at high excitation energies.

DOI: 10.1103/PhysRevC.109.064620

I. INTRODUCTION

The growing worldwide interest in the study of the nuclear fission process and fission products is due to the importance in several applications, such as the transmutation of waste produced in nuclear reactors, medicine, and network calculations in astrophysics. The fission fragment mass distributions provide fundamental information for the development of new generation reactors as well as for understanding the material damage produced by the radiation of the reactor fuel. Fission-fragment mass distributions, however, remain the key probe to study the fission mechanism, allowing the basic study of the dynamical process leading to nuclear fission [1–4].

For the spontaneous fission or fission at low excitation energies, fission fragment mass distributions are manifested by shell effects [5,6]. Indeed, the fission process is well described by the statistical model that takes into account the collective effects of nuclear deformation during fission through a liquid-drop model, and includes single-particle effects through microscopic shell-model corrections [7–9]. The microscopic corrections actually create fission valleys in the potential energy surface and each of these valleys correspond to different fission modes. With the increase in excitation energies, the role of microscopic effects diminishes, and the fission can be described by the liquid drop model (LDM). Several statistical [10,11], dynamical [12,13], microscopic [14], dinuclear system (DNS) [15,16], and semiempirical calculations [17] have been developed to produce fission-related nuclear data that are important for basic and applied nuclear physics. However, until now, such calculations were limited to lower excitation energy (<100 MeV) and angular momentum, and there exist only a few measurements at high energies [18–26] although seminal experimental studies were carried out near the Coulomb barrier energies by Itkis *et al.* [27–29]. The necessity of precise measurement at wide excitation energies and wide range of compound nuclei has been pointed out [35] for the robust interpretation of the evolution of a nucleus from the compact configuration into two fragments in a complicated multidimensional potential energy surface.

One of the reasons that the data on the systematic measurements of pure fission fragment mass distributions at high

*Contact author: tilak@vecc.gov.in

†Present address: Chanchal College, Malda, West Bengal 732123, India.

‡Present address: Argonne National Laboratory, Argonne, Illinois 60439, USA.

TABLE I. The entrance channel properties of the reactions $^{16}O + ^{181}Ta$, $^{16}O + ^{197}Au$, $^{16}O + ^{205}Tl$, and $^{16}O + ^{208}Pb$ are presented. The laboratory beam energy E_{lab}, excitation energy E^*, rotational energy E_r [30], saddle point temperature T_{SP}, average angular momentum $\langle \ell \rangle$ [31], squared of average angular momentum $\langle \ell^2 \rangle$, critical angular momentum ℓ_{cr} [32,33], the angular momentum at which the fission barrier disappears ℓ_{ff}, maximum angular momentum ℓ_{max}, and the fissility of the compound nuclei χ_{CN} [34] are tabulated.

Reaction	E_{lab} (MeV)	E^* (MeV)	E_r (MeV)	T_{SP} (MeV)	$\langle \ell \rangle$ ($\hbar$)	$\langle \ell^2 \rangle$ ($\hbar^2$)	ℓ_{cr} ($\hbar$)	ℓ_{ff} ($\hbar$)	ℓ_{max} ($\hbar$)	χ_{CN}
$^{16}O+^{181}Ta$	116	81.7	7.3	0.95	38	1444	54	68	54	0.699
	123	88.2	8.4	0.98	41	1681	59	68	61	
	130	94.6	9.7	1.01	44	1936	62	68	65	
	135	99.2	10.6	1.04	46	2116	64	68	67	
	140	103.8	11.5	1.06	48	2304	66	69	70	
	150	113.0	12.9	1.11	51	2601	69	69	74	
	155	117.6	13.9	1.13	53	2809	71	69	75	
	160	122.1	14.4	1.15	54	2916	73	69	76	
$^{16}O+^{197}Au$	116	75.0	6.1	0.90	37	1369	53	61	56	0.744
	123	81.4	7.1	0.93	40	1600	57	61	61	
	130	87.9	8.1	0.96	43	1849	61	61	65	
	135	92.5	8.9	0.98	45	2025	63	61	67	
	140	97.2	9.7	1.00	47	2209	66	62	70	
	150	106.4	11.3	1.03	50	2500	69	62	72	
	155	111.0	12.2	1.05	52	2704	71	62	75	
	160	115.7	12.6	1.07	54	2916	73	62	78	
$^{16}O+^{205}Tl$	116	64.5	5.4	0.96	36	1296	52	58	54	0.750
	123	71.0	6.7	0.99	40	1600	57	58	59	
	130	77.5	7.6	1.03	43	1849	61	58	63	
	135	82.1	8.4	1.05	45	2025	64	59	66	
	140	86.8	9.1	1.07	47	2209	66	59	69	
	150	96.1	10.7	1.10	51	2601	70	59	74	
	155	100.7	11.5	1.12	53	2809	72	59	76	
	160	105.3	11.9	1.14	54	2916	74	59	78	
$^{16}O+^{208}Pb$	116	61.2	5.3	0.98	36	1296	52	56	53	0.773
	123	67.7	6.5	1.01	40	1600	57	56	58	
	130	74.2	7.5	1.04	43	1849	61	56	63	
	135	78.9	8.2	1.06	45	2025	64	57	66	
	140	83.5	8.9	1.08	47	2209	66	57	69	
	150	92.8	10.4	1.11	51	2601	70	57	74	
	155	97.4	10.8	1.13	52	2704	72	57	76	
	160	102.0	11.7	1.14	54	2916	74	57	78	

energies is limited is that with growing excitation energies, several reaction channels open up [36,37]. Apart from the compound nuclear fission, the reaction products are an admixture of quasielastics, deep inelastic, fast fission, and quasifission events. It becomes increasingly complicated to separate fission events from other reaction products that are generated in intermediate or high-energy nuclear reactions.

The purpose of our study is to explore the fusion-fission mass distributions at excitation energies well above the Coulomb barrier with the view of obtaining a clearer understanding of the dynamics of the process. In this work, a systematic investigation was performed on the mass distributions of the fission-like events following reactions of ^{16}O beams with targets ^{181}Ta, ^{197}Au, ^{205}Tl, and ^{208}Pb. The reaction parameters are labeled in Table I. The seminal work by Toke *et al.* [21] has established that in heavy systems (e.g, ^{27}Al, ^{48}Ca, $^{48}Ti + ^{238}U$) deep-inelastic scattering, quasifission, and compound-nucleus fission may occur simultaneously. However, for lighter systems, as we have chosen in our work, the saddle is more elongated than the contact configuration, ensuring compound-nucleus fusion is likely to result when the barrier is overcome. The entrance channel charge product is much lower than the critical value (≈1600) to set in quasifission reactions. This provides the unique opportunity for a comprehensive understanding of fusion-fission process at higher energies. Our detection system was also tuned to detect the fission-like fragments while the quasielastics and deep inelastic events were transparent to the detectors. The analysis technique presented in the work efficiently separated out the noncompound (e.g., peripheral reactions like transfer induced fission, etc.) nuclear (NCN) fission events and considered only the symmetric fragments different from the projectile and target masses. Our systematic study for several preactinides nuclei and the results presented here provide benchmark data to test the new fission models at beam energies well (≈2 times) above the Coulomb barrier.

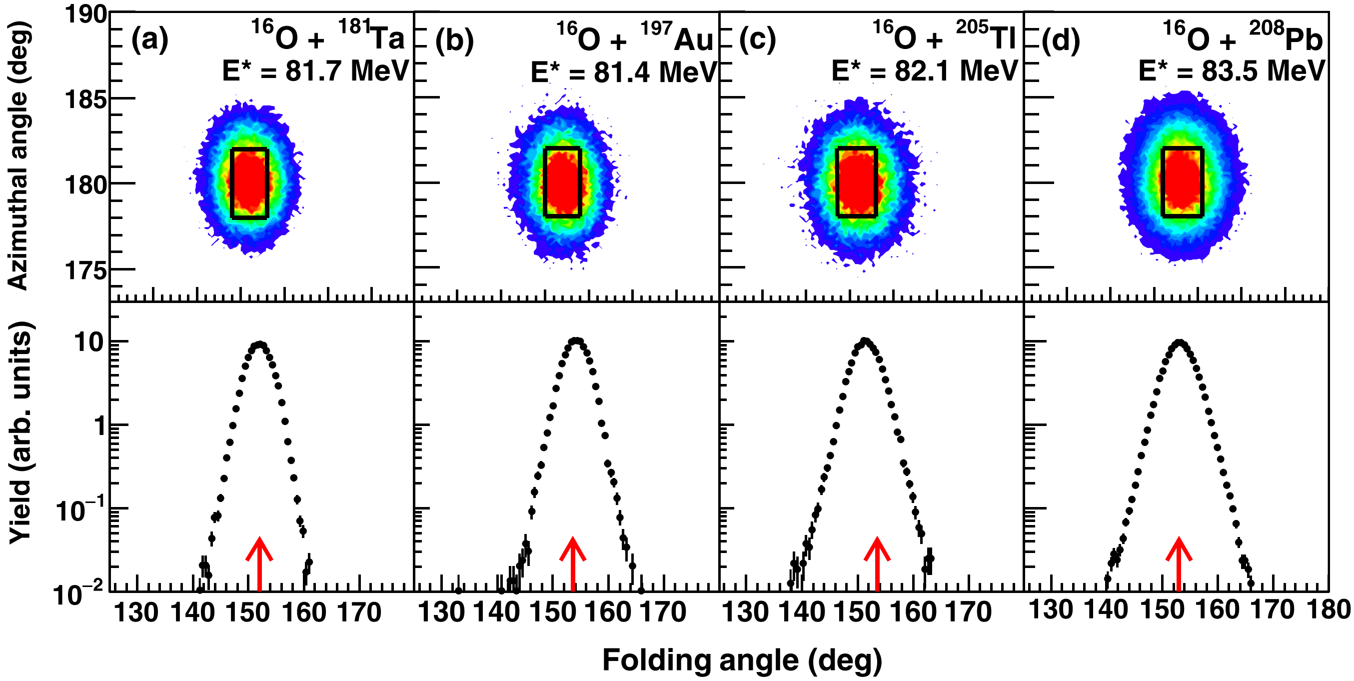

FIG. 1. The representative folding angle distributions of complementary fission fragments for the reactions $^{16}O + ^{181}Ta$, $^{16}O + ^{197}Au$, $^{16}O + ^{205}Tl$, and $^{16}O + ^{208}Pb$ at similar excitation energy of ≈81–83 MeV. We use a small rectangle gate at the center of these distributions to separate out fusion-fission events to calculate the mass distributions. The upper panel shows the (θ, ϕ) distribution whereas the bottom panel shows the folding angle distributions for the respective system. The solid red arrows in the folding angle distribution show the peak position for symmetric distribution according to the Viola's systematic [39].

II. EXPERIMENTAL DETAILS

The experiment was carried out at the K130 cyclotron facility at the Variable Energy Cyclotron Centre (VECC) in Kolkata, India. In the experiment ^{16}O beam of energies ranging from 116 to 160 MeV were bombarded on ^{181}Ta, ^{197}Au, ^{205}Tl, and ^{208}Pb targets, of thicknesses ≈300 μg/cm^2, 230 μg/cm^2, 300 μg/cm^2, and 500 μg/cm^2, respectively. The targets were positioned at an angle of 45° degrees with respect to the beam axis.

To detect the resulting fission fragments, two position-sensitive multiwire proportional counters (MWPCs) of dimension of 20 cm × 6 cm were installed inside a general-purpose scattering chamber on the two movable arms flanking the beam axis [38]. One detector was placed at a fixed angle of 90° at a distance of 35.5 cm from the target, while the other detector, kept at 29.9 cm, was rotated corresponding to the folding angle during the change in beam energy. The detectors were operated with isobutane gas at a 3 torr pressure so that the quasielastic and majority of the deep inelastic particles may pass through without producing a detectable signal. The low gas pressure was helpful to ensure that the low mass deep inelastic events were transparent and the clean identification of the fusion fission events could be achieved.

Using a VME-based data acquisition system, the position information (X, Y), energy loss in the detectors, and time of flight of the binary fragments with respect to the pulsed beam were recorded event by event. The complementary fragments masses were determined using the time-of-flight (TOF) difference method. The X and Y coordinates of the MWPCs were calibrated using a ^{252}Cf source, and the emission angle for each fragment was calculated using this calibration. Counts from the Faraday cup were utilized for beam flux monitoring as well as data normalization. The experimental setup had a mass resolution (FWHM) of ≈5 u. The procedure for the determination of the fission fragment mass distribution is reported in our earlier reports [38,40–42].

III. RESULTS AND DISCUSSIONS

From the measured time-of-flight difference and position information, the fission-fragment folding angle and mass distributions were determined.

A. Folding angle distributions

The fission fragments originating from the complete fusion-fission events can be separated [43] from the non-compound nuclear fission (e.g., transfer fission) using the distributions of polar (θ) and azimuthal (ϕ) angles of the detected fragments; as well as from the correlation of the velocities of the fissioning system in the beam direction (V_{para}) and perpendicular to the reaction plane (V_{perp}). The typical fission fragment folding angle distributions in the reaction plane (θ) vs. out of the plane (ϕ) is shown in Figs. 1(a)–1(d) in the upper panel; the bottom panel of the figure shows the projections of the folding angles onto the reaction plane. The peaks of the folding angle distributions are found to be consistent with the predicted values (as indicated by the solid red arrow in the bottom panel of Fig. 1) for the complete

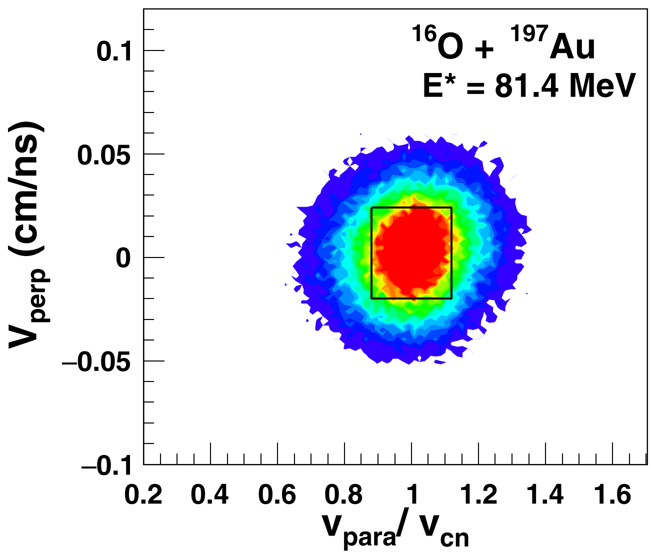

FIG. 2. A representative plot of the correlation of velocity distribution in the parallel and perpendicular to the beam axis. The gate at the excitation energy $E^* = 81.4$ MeV is shown by the black contour for the selection of fusion-fission events from inclusive events in the reaction $^{16}O + ^{197}Au$.

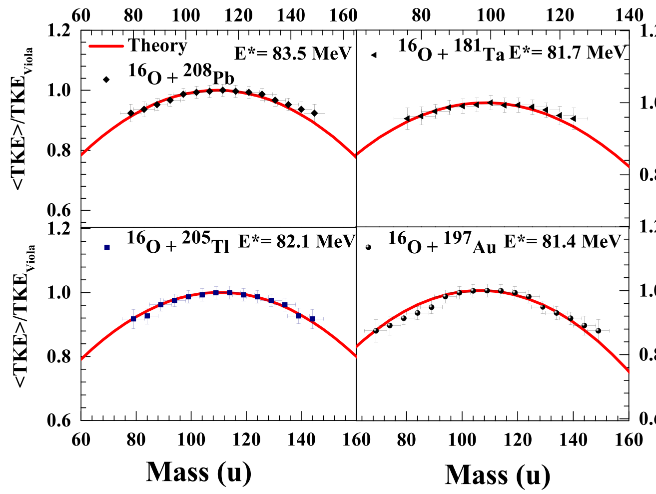

FIG. 3. The variation of average TKE with mass for the reactions $^{16}O + ^{181}Ta$, $^{16}O + ^{197}Au$, $^{16}O + ^{205}Tl$, and $^{16}O + ^{208}Pb$ obtained at excitation energy $E^* \approx 83$ MeV. The parabolic dependency described in Eq. (1) is represented by the solid red curve.

momentum transfer of the projectile. The folding angle distribution with the peak consistent with the calculated value is indicative of a complete transfer of projectile momentum and minimal absence of transfer fission events. Nevertheless, the width of the polar and azimuthal angular correlations are wider owing to the intricate interplay of fusion-fission reaction kinematics, as well as admixture of fission like events and the dispersion is also caused by post-scission neutron emission from the fragments.

A representative correlation plot between parallel and perpendicular components of velocity distributions ($V_{\text{para}}, V_{\text{perp}}$) is shown in Fig. 2 at an excitation energy of 81.4 MeV for the reaction $^{16}O + ^{197}Au$. A clear distinction between complete fusion (CF) fission reaction and NCN reaction is not prominent in Figs. 1 and 2. Therefore, we *select* only the intense peak at the center that corresponds to the CF events. We used a narrow gate, as shown by black contours, to select the possible CF events. It has been checked that a more narrow gate only reduces the statistics but does not have effect on the mass distribution width.

B. Mass-TKE distributions

Apart from the folding angle, the mass-total kinetic energy (M-TKE) distributions provide information about the nature of the reaction process. In the case of the pure fusion-fission process, the TKE of fission fragments is independent of CN excitation energy and follows a relationship on fragment mass (M):

$$\text{TKE}(M) = 4 \times \text{TKE}_{\text{Viola}} \times \frac{M(M_{CN} - M)}{M_{CN}^2}, \tag{1}$$

where $\text{TKE}_{\text{Viola}}$ is the most probable TKE estimated using the Viola systematic [39]. Figure 3 shows the M-TKE distributions of the selected (as shown by black boxes in Figs. 1 and 2) binary fragments produced in the reactions $^{16}O + ^{181}Ta$, $^{16}O + ^{197}Au$, $^{16}O + ^{205}Tl$, and $^{16}O + ^{208}Pb$ at a representative excitation energy of $E^* \approx 81$–83 MeV. The parabolic variation of average TKE with mass as shown in Fig. 3, consistent with LDM, also indicates that the selected events in our analysis follow fusion-fission path up to the measured excitation energies, and there is no admixture of noncompound nuclear fission.

C. Mass-angle correlations

At high excitation energies, several noncompound nuclear processes are expected to contribute to the detected fragments. Quasifission time scale is believed to be intermediate between deep-inelastic scattering and fission of the fully equilibrated compound nucleus. In the case of quasifission reactions, since the composite system breaks before a full rotation is completed, there exists a correlation between the mass and angle of the fragments [2]. In order to check if there are quasifission events in the detected fragments, the mass-angle correlation for the reactions $^{16}O + ^{181}Ta$, $^{16}O + ^{197}Au$, $^{16}O + ^{205}Tl$, and $^{16}O + ^{208}Pb$ obtained at a representative excitation energy of $E^* \approx 81$–83 MeV is shown in Fig. 4 for the selected events (as discussed in Figs. 1 and 2) for which mass distributions have been analyzed. No significant correlation of fragment mass with angle was observed, indicating the absence of quasifission events in the selected events of our analysis.

D. Mass distributions

Figure 5 shows the typical mass distributions of fission fragments for the selected events in the reactions $^{16}O + ^{181}Ta$, $^{16}O + ^{197}Au$, $^{16}O + ^{205}Tl$, and $^{16}O + ^{208}Pb$ at different excitation energies well above the Coulomb barrier. The distributions exhibit a symmetrical nature, with peaks located near half of the combined mass of the target and projectile, i.e.,

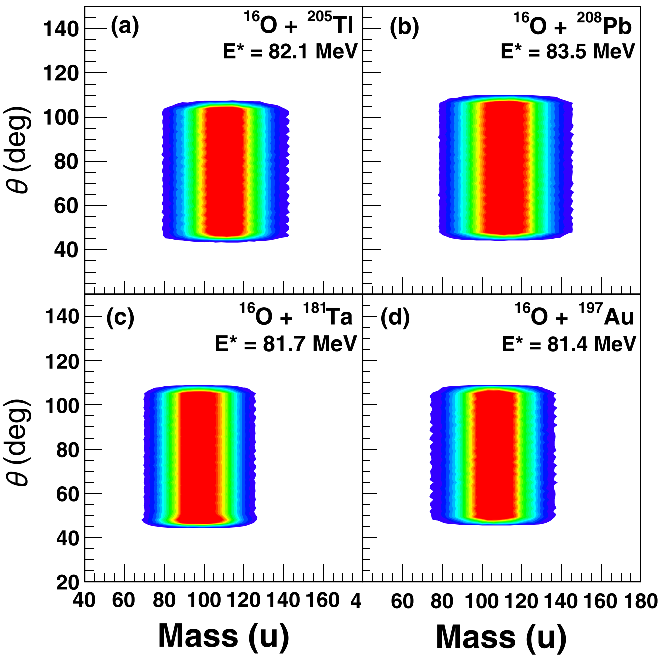

FIG. 4. The mass-angle correlation for the reactions ^{16}O + ^{181}Ta, ^{16}O + ^{197}Au, ^{16}O + ^{205}Tl, and ^{16}O + ^{208}Pb obtained at similar excitation energy.

$\approx A_{CN}/2$. The solid (red) line represents a single Gaussian fit that matches the experimental data well and indicates no significant inclusion of asymmetric distribution.

In Fig. 6, the variation of standard deviation $\sigma_m(u)$ of the fitted experimental mass distributions is shown as a function of excitation energy. For all the reactions ^{16}O + ^{181}Ta, ^{16}O + ^{197}Au, ^{16}O + ^{205}Tl, and ^{16}O + ^{208}Pb, the standard deviation $\sigma_m(u)$ exhibits a smooth increase with excitation energy.

To gain further insights into the nature of the observed mass distributions, we focus our attention on the width of these distributions. The width of the mass distribution in the statistical model of fusion-fission is determined by two factors: the saddle point temperature (T) and the mean squared angular momentum $\langle\ell^2\rangle$ of the fissioning system. The standard deviation of the mass distribution in the statistical model of fission can be described by the following expression:

$$\sigma_m(u) = \sqrt{\alpha T + \beta\langle\ell^2\rangle}, \tag{2}$$

where $\alpha = 1/k$; k is the stiffness parameter of the nucleus along the mass-asymmetry, and β is a constant. The calculated mass width is sensitive to the used temperature. Since the saddle-to-scission path is short for the nuclei under study [44], consideration of saddle point temperature is justified. The temperature is calculated using the relation [10]

$$T_{\text{saddle}} = \left(\frac{E_{\text{mid}} - B_f(\ell) - E_n}{a}\right)^{1/2}, \tag{3}$$

where $E_{\text{mid}} = E^* - E_{\text{rot}}^{gs}(\ell)$ is the excitation energy after subtracting the ℓ-dependent rotational energy of the nucleus in the ground state $E_{\text{rot}}^{\text{g.s.}}(\ell)$ [30]. The initial excitation energy $E^*(= E_{\text{c.m.}} + Q)$ is the sum of the energy in the center of mass ($E_{\text{c.m.}}$) frame of reference and the Q value for the formation of the CN. $B_f(\ell)$ is the ℓ-dependent fission barrier. $B_f(\ell)$ and $E_{\text{rot}}^{\text{g.s.}}(\ell)$ were calculated by the rotating finite range model (RFRM) of Sierk [30]. The average energy removed by the evaporated neutrons from the CN is denoted by E_n, which was obtained by the following relation:

$$E_n = \langle\nu_{\text{pre}}\rangle \times (B_n + \langle E_{\text{kin}}\rangle), \tag{4}$$

where B_n is the neutron binding energy, $\langle\nu_{\text{pre}}\rangle$ were calculated from the systematics [10,45]. $\langle E_{\text{kin}}\rangle = 2T_{\text{mid}}$ is the average kinetic energy carried away by the neutrons [46]. $T_{\text{mid}} = \sqrt{E_{\text{mid}}/a}$ is the temperature of nuclei at excitation energy E_{mid}. A level density parameter of $a = A/8.5$ was used in the calculation [20,22]. The angular momentum $\langle\ell\rangle$ of the compound nucleus (CN) was determined using the CCFULL code [31]. The Woods-Saxon parametrization of the Akyüz-Winther potential [47] was employed for the three components of the nuclear potential utilized in CCFULL. These components include the depth V_0, the radius r_0, and the diffuseness parameter a.

The calculated value of $\sigma_m(u)$ using Eq. (2) with a value of the inverse stiffness parameter $\alpha(= 1/k) = (98.1 \pm 15.1)$ u^2/MeV [44] is shown by the solid red lines in Fig. 6 and was found to fit the experimental data well for all the systems in the present measurement. The same value of α were found to explain the mass distribution data at low excitation energies [48]. The parameter α characterizes the stiffness of the nuclear potential and is predicted [49–51] to have dependence upon nuclear temperature and angular momentum. Our measurement indicate the weak dependence of the inverse stiffness parameter up to the measured excitation energy range ($\approx$120 MeV).

The calculations have been executed for all the systems within the energy range under investigation, employing the semiempirical code GEF [17]. This code has effectively elucidated mass distributions of fission fragments for various nuclei at lower excitation energies ($\leqslant$ 60 MeV) [35]. We have applied this code to contrast the experimental data from our present measurements, conducted at higher excitation energies and angular momentum. As shown in Fig. 6, the calculation from GEF predict a significantly higher width compared to the experimental values. This deficiency of the calculation can probably be attributed to the restrictions of the model and the parameters of the semiempirical code was not benched marked at higher excitation energies.

Since the saddle point model calculation explains the data well but not by GEF, which considers shell corrections at the saddle, another analysis has been carried out as proposed by Itkis *et al.* [24,27–29] where the transitional-state method with shell correction is utilized in characterizing the mass distribution. The fragment mass distributions can be expressed as

$$Y(M) \sim \exp\left\{-\frac{\alpha}{2T}(M - A/2)^2 - \frac{\delta W_f(M)}{T}\exp(-\lambda U)\right\}, \tag{5}$$

where α is the stiffness parameter of the liquid-drop model of the nucleus with respect to mass-asymmetric variations of the saddle-point shape, T is the temperature of the nucleus at the saddle point, and U is the energy at saddle. Here,

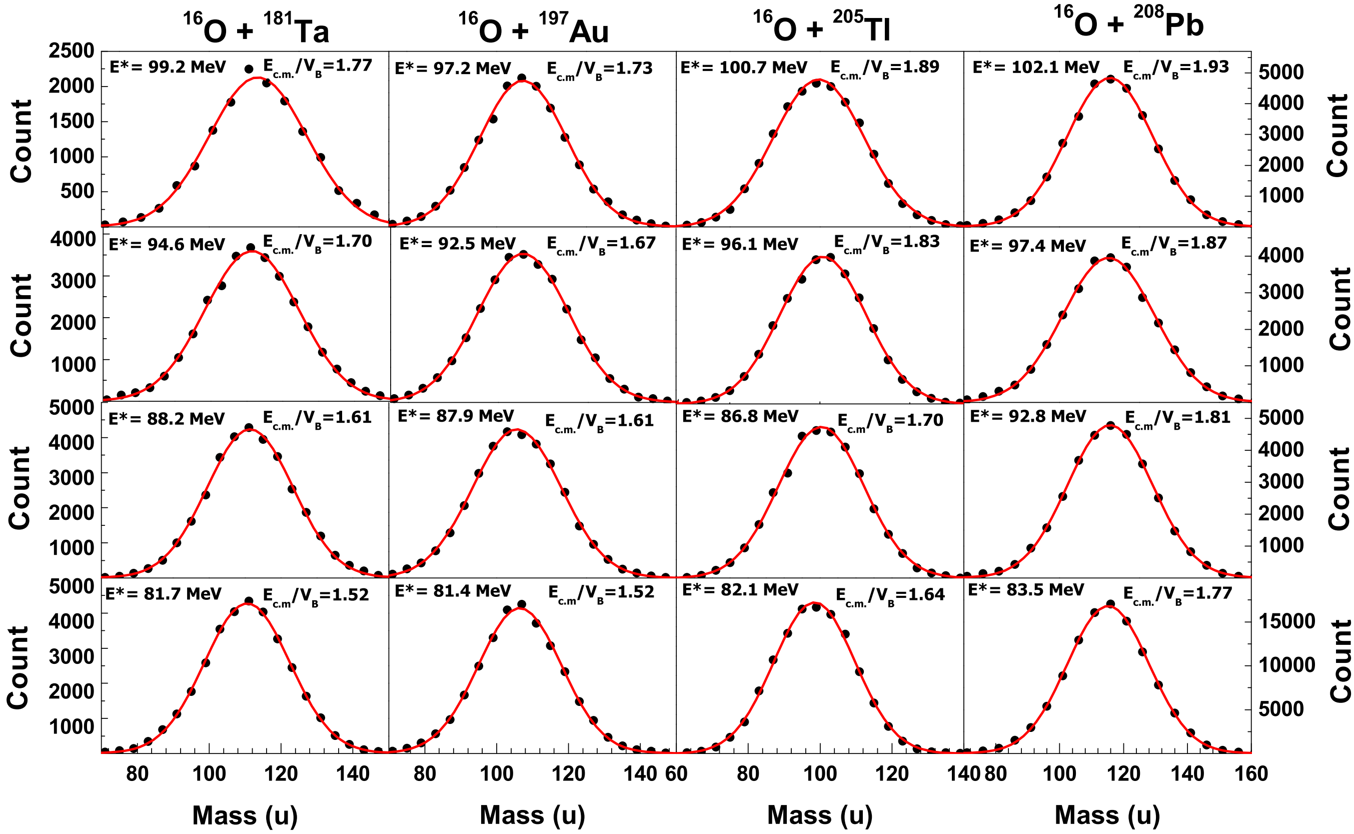

FIG. 5. Experimental mass distributions of fission fragments for the four reactions $^{16}O + ^{181}Ta$, $^{16}O + ^{197}Au$, $^{16}O + ^{205}Tl$, and $^{16}O + ^{208}Pb$ at different excitation energies. The distributions were fitted by a single Gaussian, shown by full (red) lines.

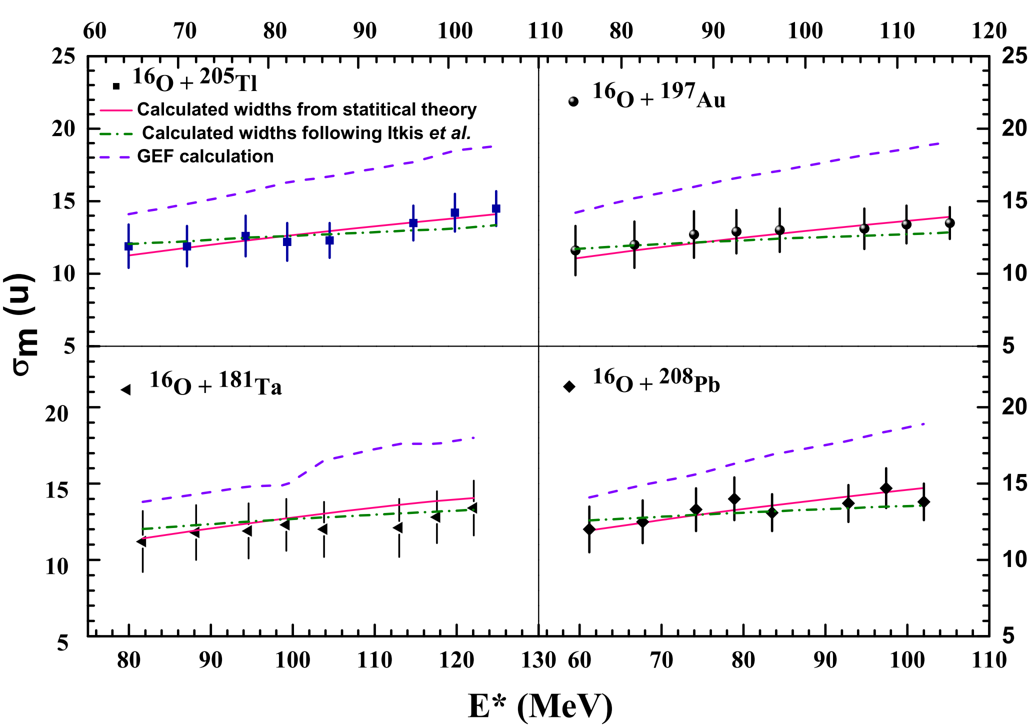

FIG. 6. Variation of the measured standard deviation $\sigma_m(u)$ of the mass distributions with excitation energy. The calculated $\sigma_m(u)$ following statical theory and Itkis's prescription are shown by solid and dashed-dotted lines, respectively, as described in the text. GEF calculations are shown by the dashed lines.

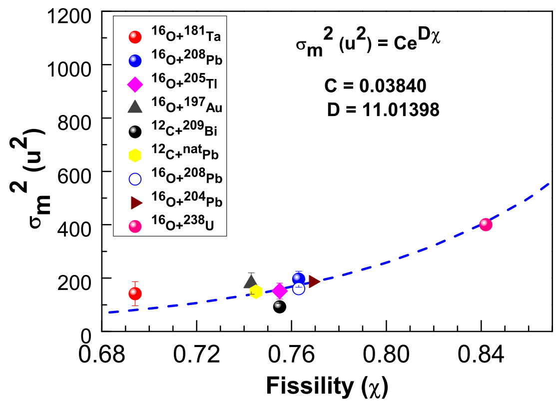

FIG. 7. Variation of mass variance (σ_m^2) as a function of fissility of the compound nuclei populated in reactions ^{16}O + ^{181}Ta, ^{16}O + ^{197}Au, ^{16}O + ^{205}Tl, ^{16}O + ^{208}Pb in the present study along with the literature data for the reactions ^{12}C + ^{209}Bi, ^{12}C + $^{\rm nat}$Pb, ^{16}O + ^{208}Pb, ^{16}O + ^{204}Pb [52], and ^{16}O + ^{238}U [42]. The dashed line indicate fitting with two-parameter exponential equation with the best fitted value of the parameters.

$\lambda = 0.064\,\mathrm{MeV}^{-1}$ and δW_f is the shell correction, which is localized in a rather narrow region $M \sim A/2$, can be written as

$$\delta W_f = \delta W_f(A/2)\exp[-\gamma(M - A/2)^2]. \tag{6}$$

Here, $\gamma = 0.015$–0.02 amu^{-2}. Equation (5) contains two parts; the first term originates from the liquid drop model, while the shell correction is taken care by the second term. The shell correction factor in Eq. (5) is calculated using Eq. (6), with the value of $\delta W_f(A/2)$ is between $+1$ to -1. All the measured mass distributions were fitted with Eq. (5), and $\sigma_m(u)$ was calculated. While fitting the mass distributions, the magnitude of the shell effect was found to decrease with increasing excitation energy, as expected. As can be seen in Fig. 6 that the variation of $\sigma_m(u)$ with excitation energy (shown by dot-dashed line) is also consistent with experimental data.

E. Fissility dependence of mass variance

The variation of the variance of mass distribution σ_m^2(u) as a function of fissility has been plotted in Fig. 7 for the studied reactions at a fixed compound nuclear temperature 1.06 MeV. Apart from our present measurement, data existing in the literature [42,52] have also been used. The data could be well fitted by the two-parameter exponential equation as shown by the dashed line in Fig. 7. The exponential dependence of $\sigma_m^2(u)$ on fissility also supports the compound nuclear behavior of the measured reactions. Similar kind of fissility dependence of mass variance was reported by Sawant *et al.* [52] and Oganessian *et al.* [53] at a saddle point temperature of 1.5 MeV.

F. Fast fission

Since the measurements were carried out well above the Coulomb barrier energies, we critically examined the presence of any events other than the complete fusion-fission reactions. The angular correlation between the detected fragments can also be used as a tool to study the reaction mechanism. The emission angle of the fragments is influenced by their kinetic energies and reflected in the actual angular correlations of the fragments. The kinetic energies of the fragments are decided by the dissipation of energies during the passage from the contact configuration to scission.

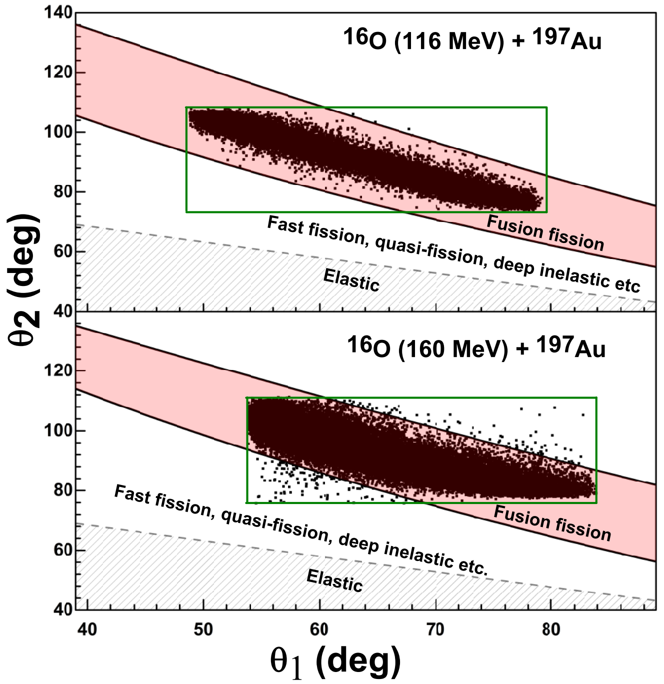

FIG. 8. A representative correlation plot of the simulated polar angle distributions of the events produced in the reaction ^{16}O + ^{197}Au at the lowest (116 MeV) and highest beam energy (160 MeV) measured in the experiment. The shaded area indicates that the symmetric and asymmetric (up to a ratio of 3 : 1 in mass) fusion-fission events are expected to be contained in this region. The elastic events are expected to be in the hatched region, while the less dissipative events (like deep inelastic collision, fast fission, or quasifission, etc.) should lie above hatched region. The detector coverage is shown by the green rectangular box. The measured events are shown by the black dots.

Figure 8 shows the simulated polar angle correlation of the typical fusion-fission, deep-inelastic, fast fission, quasifission, and elastics events at the lowest (116 MeV) and highest (160 MeV) energies of our measurements for the reaction ^{16}O + ^{197}Au. The shaded region shows the expected fusion-fission events following the complete transfer of momentum from the projectile to the target. The folding angle was calculated for symmetric and asymmetric (up to a mass ratio of 3 : 1) fission events using Viola's systematic [39]. The detected events in the experiment are shown in the figure by black dots. The elastic events should lie in the hatched region while the events originating from the less dissipative events (e.g., deep inelastic collision, fast fission, or quasifission) are expected to be contained above the hatched region, as indicated in the figure. The large angular coverage of the detector used in the experiment,

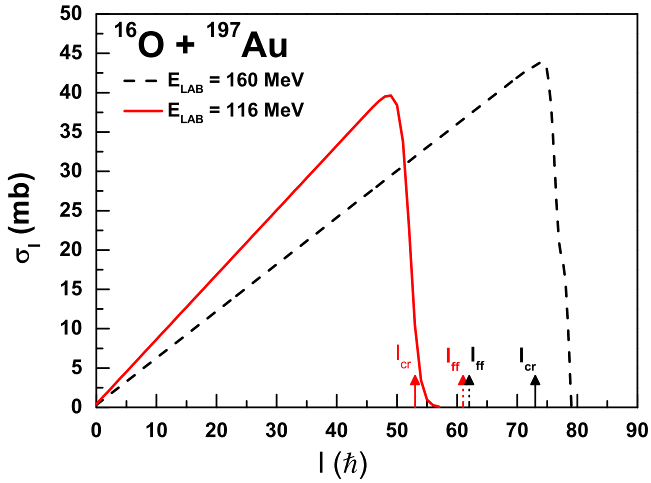

FIG. 9. Partial capture cross sections as a function of angular momentum for the ^{16}O + ^{197}Au reaction at 116 MeV and 160 MeV. The critical angular momentum (l_{cr}) and the values of the angular momentum (l_{ff}) at which fast fission appears at the respective energies are indicated in the figure.

shown by the solid green rectangular contour, ensured the detection of all the fission-like fragments. It is interesting to observe that the data from the reaction at a laboratory energy of 116 MeV falls well within the region of the predicted fusion fission events. However, for the $E_{\rm Lab} = 160$ MeV data, a number of events were observed outside the predicted range of fusion-fission and lie in the region that corresponds to less dissipative events (e.g., deep inelastic collision, fast fission, or quasifission) for which the total kinetic energy of the fragments are different from that following Viola's systematic.

Figure 9 shows the representative partial capture cross sections as a function of angular momentum for the ^{16}O + ^{197}Au reaction at 116 MeV and 160 MeV. The partial capture cross sections were calculated within the coupled channels approach. The critical angular momentum (l_{cr}) at which fusion pocket vanishes and the value of the angular momentum (l_{ff}) at which fission pocket disappears are indicated in the figure. According to the conventional picture of heavy ion reactions, compound nuclear reaction occurs for $0 < l < l_{ff}$. Deep inelastic events are observed for $l > l_{cr}$ and for $l > l_{ff}$ fast fission is expected to contribute in the reaction process. The figure suggests that deep inelastic events may contribute both at the 116 MeV and 160 MeV energies, but fast fission will contribute at 160 MeV. As the detectors were operated at low gas pressure, low mass deep inelastic events were not observed in the measurements. However, fast fission events that are similar to fusion fission events in mass could be detected. Quasifission are unlikely for systems under study with low entrance channel charge product and mainly contribute to the capture cross section at energies near the Coulomb barrier [5]. Thus at 116 MeV the observed events are fusion fission events and there could be the presence of fast fission events at 160 MeV.

To further clarify that the events located outside the fusion-fission region as indicated in Fig. 8 at 160 MeV are originated from the fast fission process, we carried out the following

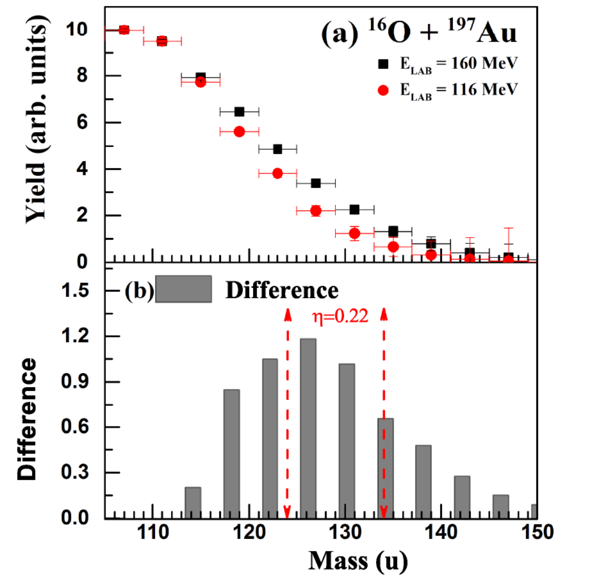

FIG. 10. (a) The fission fragment half-mass distributions at the lowest (116 MeV) and highest (160 MeV) energies of our measurement for the ^{16}O + ^{197}Au reaction. (b) The extracted difference between the mass distributions are found to peak at the mass asymmetry $\eta = (M_H - M_L)/(M_H + M_L) \approx 0.22$.

analysis. In Fig. 10(a) we show the representative plot of the half-mass distributions for all the events measured in the ^{16}O + ^{197}Au reaction at 160 MeV and 116 MeV beam energy. The difference of these distributions, as shown in Fig. 10(b) indicates an asymmetric component with the mass asymmetry $\eta = (M_H - M_L)/(M_H + M_L) \approx 0.22$. Previous studies [54] suggested that this component with the observed mass asymmetry value is manifested in the fast fission process.

It is known that the width of the mass distribution for fast fission are wider compared to the fusion fission process. In Fig. 11 we show the standard deviation of the mass distributions for all the measured systems at 160 MeV. The

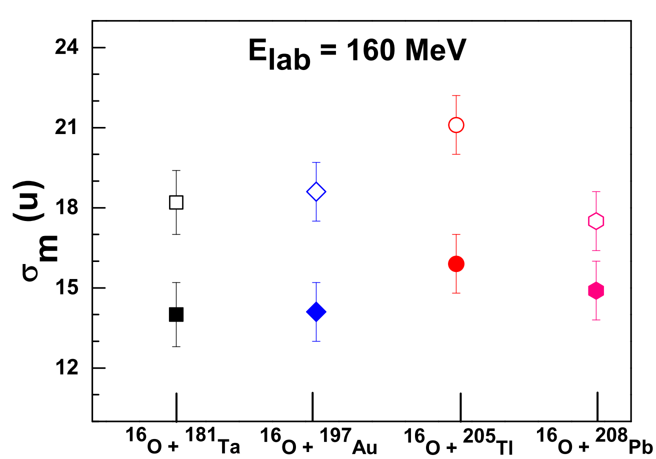

FIG. 11. The open symbols shows the standard deviation of the fragment mass distribution for the less dissipative events and the solid points are for the events contained in the fusion-fission region at 160 MeV for the all four reactions studied in this work.

hollow points indicate the standard deviation of mass distributions of the events outside the shaded (fusion-fission) region as shown in the representative Fig. 8 for the $^{16}O + ^{197}Au$ reaction. It can be observed that the observed standard deviations are significantly higher than the standard deviations of the fragment mass distributions for the events contained in the fusion-fission region. The above analysis clearly suggests the presence of fast fission events at 160 MeV.

IV. SUMMARY AND CONCLUSION

To sum up, we have presented systematic measurements of fission-fragment mass distributions in the large entrance channel mass asymmetric reactions $^{16}O + ^{181}Ta$, ^{197}Au, ^{205}Tl, and ^{208}Pb over a wide energy range, well above the Coulomb barrier, providing insight on the dynamics of the fission process. The fission fragment mass distributions for all the systems studied from the carefully selected events, were found to be predominantly symmetric Gaussian, with peaks located near half of the combined mass of the target and projectile. The variance of the mass distributions monotonically increase with excitation energy, consistent within the framework of statistical model predictions, though significantly deviate compared to semiempirical calculation. The variation of average total kinetic energy with mass showed a parabolic dependence supporting the liquid drop model behavior in the measured energy range. The measured variation of the variance of the mass distribution with the fissility showed an exponential increase is consistent with liquid drop model behavior. The results demonstrate that fissioning nucleus distributions are consistent with statistical model predictions for reactions well above the Coulomb barrier energies. Our measurements indicate the weak dependence of the inverse stiffness parameter up to the measured excitation energy range. The analysis has shown the presence of fast fission events at the higher excitation energy characterized by a mass asymmetry 0.22. The systematic measurement presented in this work for a wide range of energy and several preactinide target nuclei provides benchmark data to test the new reaction models above the Coulomb barrier energies.

ACKNOWLEDGMENTS

The authors express their sincere thanks to the accelerator staff at VECC Kolkata for providing high-quality beams for the experiment. We would also like to thank J. K. Meena, A. K. Saha, J. K. Sahoo, S. Dalal, and R. M. Saha for their assistance during the experiment. We are thankful to Dr. S. Bhattacharya for a critical reading of the manuscript.

[1] A. N. Andreyev, K. Nishio, and K.-H. Schmidt, Rep. Prog. Phys. **81**, 016301 (2018).
[2] D. J. Hinde, M. Dasgupta, and E. C. Simpson, Rep. Prog. Phys. **118**, 103856 (2021).
[3] T. K. Ghosh, S. Pal, T. Sinha, S. Chattopadhyay, P. Bhattacharya, D. C. Biswas, and K. S. Golda, Phys. Rev. C **70**, 011604(R) (2004).
[4] R. Leguillona, K. Nishio, K. Hirose *et al.*, Phys. Lett. B **761**, 125 (2016).
[5] M. G. Itkis, E. Vardaci, I. M. Itkis, G. N. Knyazheva, and E. M. Kozulin, Nucl. Phys. A **944**, 204 (2015).
[6] A. Chaudhuri, T. K. Ghosh *et al.*, Phys. Rev. C **91**, 044620 (2015).
[7] A. Chaudhuri, T. K. Ghosh *et al.*, Phys. Rev. C **92**, 041601(R) (2015).
[8] D. Paul, A. Sen, T. K. Ghosh *et al.*, Phys. Rev. C **104**, 024604 (2021).
[9] E. Andrade-II *et al.*, J. Phys. G: Nucl. Part. Phys. **38**, 085104 (2011).
[10] M. G. Itkis and A. Y. Russanov, Phys. Part. Nucl. **29**, 160 (1998).
[11] F. Gonnenwein, *The Nuclear Fission Process* (CRC Press, Boca Raton, FL, 1991),
[12] P. Möller and J. Randrup, Phys. Rev. C **91**, 044316 (2015).
[13] M. R. Mumpower, P. Jaffke, M. Verriere, and J. Randrup, Phys. Rev. C **101**, 054607 (2020).
[14] N. Schunck and L. M. Robledo, Rep. Prog. Phys. **79**, 116301 (2016).
[15] A. K. Nasirov *et al.*, Phys. Lett. B **842**, 137976 (2023).
[16] G. Fazio, G. Giardina, G. Mandaglio, R. Ruggeri, A. I. Muminov, A. K. Nasirov, Y. T. Oganessian, A. G. Popeko, R. N. Sagaidak, A. V. Yeremin, S. Hofmann, F. Hanappe, and C. Stodel, Phys. Rev. C **72**, 064614 (2005).
[17] K.-H. Schmidt, B. Jurado, C. Amouroux, and C. Schmitt, Nucl. Data Sheets **131**, 107 (2016).
[18] R. Bock, Y. T. Chu, M. Dakowski, A. Gobbi, E. Grosse, A. Olmi, H. Sann, D. Schwalm, U. Lynen, W. Müller, S. Bjørnholm, H. Esbensen, W. Wolfli, and E. Morenzoni, Nucl. Phys. A **388**, 334 (1982).
[19] B. G. Glagola, B. B. Back, and R. R. Betts, Phys. Rev. C **29**, 486 (1984).
[20] B. B. Back, R. R. Betts, J. E. Gindler, B. D. Wilkins, S. Saini, M. B. Tsang, C. K. Gelbke, W. G. Lynch, M. A. McMahan, and P. A. Baisden, Phys. Rev. C **32**, 195 (1985).
[21] J. Tōke *et al.*, Nucl. Phys. A **440**, 327 (1985).
[22] W. Q. Shen *et al.*, Phys. Rev. C **36**, 115 (1987).
[23] D. J. Hinde, D. Hilscher, H. Rossner, B. Gebauer, M. Lehmann, and M. Wilpert, Phys. Rev. C **45**, 1229 (1992).
[24] M. G. Itkis *et al.*, Yad. Fiz. **43**, 1125 (1986).
[25] M. G. Itkis *et al.*, Nucl. Phys. A **734**, 136 (2004).
[26] K. Atreya, A. Sen, T. K. Ghosh *et al.*, Phys. Rev. C **108**, 034615 (2023).
[27] M. G. Itkis *et al.*, Yad. Fiz. **52**, 23 (1990).
[28] M. G. Itkis *et al.*, Sov. J. Part. Nucl. **19**, 301 (1988).
[29] M. G. Itkis *et al.*, Yad. Fiz. **53**, 1225 (1991).
[30] A. J. Sierk, Phys. Rev. C **33**, 2039 (1986).
[31] K. Hagino, N. Rowley, and A. J. Kruppa, Comput. Phys. Commun. **123**, 143 (1999).
[32] R. J. Charity, L. G. Sobotka, J. Cibor, K. Hagel, M. Murray, J. B. Natowitz, R. Wada, Y. El Masri, D. Fabris, G. Nebbia, G. Viesti, M. Cinausero, E. Fioretto, G. Prete, A. Wagner, and H. Xu, Phys. Rev. C **63**, 024611 (2001).

[33] D. Mancusi, R. J. Charity, and J. Cugnon, Phys. Rev. C **82**, 044610 (2010).
[34] J. P. Blocki, H. Feldmeier, and W. J. Swiatecki, Nucl. Phys. A **459**, 145 (1986).
[35] C. Schmitt, K. Mazurek, and P. N. Nadtochy, Phys. Rev. C **97**, 014616 (2018).
[36] H. Feldmeier, Rep. Prog. Phys. **50**, 915 (1987).
[37] E. Vardaci *et al.*, Phys. Rev. C **101**, 064612 (2020).
[38] T. K. Ghosh *et al.*, Nucl. Instrum. Methods Phys. Res. A **540**, 285 (2005).
[39] V. E. Viola, K. Kwiatkowski, and M. Walker, Phys. Rev. C **31**, 1550 (1985).
[40] T. K. Ghosh *et al.*, Phys. Lett. B **627**, 26 (2005).
[41] T. K. Ghosh, S. Pal, T. Sinha, N. Majumdar, S. Chattopadhyay, P. Bhattacharya, A. Saxena, P. K. Sahu, K. S. Golda, and S. K. Datta, Phys. Rev. C **69**, 031603(R) (2004).
[42] D. Paul, Ph.D. thesis, The Homi Bhabha National Institute, 2023.
[43] D. J. Hinde, M. Dasgupta, J. R. Leigh, J. C. Mein, C. R. Morton, J. O. Newton, and H. Timmers, Phys. Rev. C **53**, 1290 (1996).
[44] G. N. Knyazheva, E. M. Kozulin *et al.*, Phys. Rev. C **75**, 064602 (2007).
[45] E. M. Kozulin, A. Y. Rusanov, and G. N. Smirenkin, Yad. Fiz. **56**, 37 (1993) [Phys. At. Nucl. **56**, 166 (1993)].
[46] I. V. Pokrovsky, L. Calabretta, M. G. Itkis, N. A. Kondratiev, E. M. Kozulin, C. Maiolino, E. V. Prokhorova, A. Ya. Rusanov, and S. P. Tretyakova, Phys. Rev. C **60**, 041304(R) (1999).
[47] R. A. Broglia and A. Winther, *Heavy Ion Reactions* (Benjamin-Cummings, Reading, MA, 1981), Vol. 1.
[48] A. Chaudhuri, A. Sen, T. K. Ghosh, K. Banerjee, J. Sadhukhan, S. Bhattacharya, P. Roy, T. Roy, C. Bhattacharya, M. A. Asgar, A. Dey, S. Kundu, S. Manna, J. K. Meena, G. Mukherjee, R. Pandey, T. K. Rana, V. Srivastava, R. Dubey, G. Kaur, N. Saneesh, P. Sugathan, and P. Bhattacharya, Phys. Rev. C **94**, 024617 (2016).
[49] C. Ngô, C. Gregoire, B. Remaud, and E. Tomasi, Nucl. Phys. A **400**, 259 (1983).
[50] C. Gregoire, C. Ngo, E. Tomasi, B. Remaud, and F. Scheuter, Nucl. Phys. A **387**, 37 (1982).
[51] M. Faber, Report No. AIAU-8023, Wien (1980).
[52] Y. S. Sawant, A. Saxena, R. K. Choudhury, P. K. Sahu, R. G. Thomas, L. M. Pant, B. K. Nayak, and D. C. Biswas, Phys. Rev. C **70**, 051602(R) (2004).
[53] Y. T. Oganessian and Y. A. Lazarev, in *Treatise on Heavy Ion Science*, edited by D. A. Bromley (Plenum Press, New York, 1985), Vol. 4, p. 1.
[54] E. M. Kozulin, G. N. Knyazheva *et al.*, Phys. Rev. C **105**, 024617 (2022).